Materials Science and Engineering C 62 (2016) 497–505

Contents lists available at ScienceDirect

Materials Science and Engineering C

journal homepage: www.elsevier.com/locate/msec

Dissolution behaviour of silicon nitride coatings for joint replacements

Maria Pettersson [a], Michael Bryant [b], Susann Schmidt [c], Håkan Engqvist [a], Richard M. Hall [d], Anne Neville [b], Cecilia Persson [a,*]

[a] Materials in Medicine Group, Div. of Applied Materials Science, Dept. of Engineering Sciences, Uppsala University, Uppsala, Sweden
[b] Institute of Functional Surfaces (iFS), School of Mechanical Engineering, University of Leeds, Leeds, United Kingdom
[c] Thin Film Physics, Department of Physics, Chemistry and Biology (IFM), Linköping University, Linköping, Sweden
[d] Institute of Medical and Biological Engineering (iMBE), School of Mechanical Engineering, University of Leeds, Leeds, United Kingdom

ARTICLE INFO

Article history:
Received 4 November 2015
Received in revised form 11 January 2016
Accepted 20 January 2016
Available online 22 January 2016

Keywords:
Silicon nitride
Cobalt chromium
Coating
Dissolution
Corrosion
Mass loss
Joint replacement

ABSTRACT

In this study, the dissolution rate of SiN_x coatings was investigated as a function of coating composition, in comparison to a cobalt chromium molybdenum alloy (CoCrMo) reference. SiN_x coatings with N/Si ratios of 0.3, 0.8 and 1.1 were investigated. Electrochemical measurements were complemented with solution (inductively coupled plasma techniques) and surface analysis (vertical scanning interferometry and x-ray photoelectron spectroscopy). The dissolution rate of the SiN_x coatings was evaluated to 0.2–1.4 nm/day, with a trend of lower dissolution rate with higher N/Si atomic ratio in the coating. The dissolution rates of the coatings were similar to or lower than that of CoCrMo (0.7–1.2 nm/day). The highest nitrogen containing coating showed mainly Si–N bonds in the bulk as well as at the surface and in the dissolution area. The lower nitrogen containing coatings showed Si–N and/or Si–Si bonds in the bulk and an increased formation of Si–O bonds at the surface as well as in the dissolution area. The SiN_x coatings reduced the metal ion release from the substrate. The possibility to tune the dissolution rate and the ability to prevent release of metal ions encourage further studies on SiN_x coatings for joint replacements.

1. Introduction

Whilst some modern total hip replacements have a high success rate of 97.8% after 10 years [1], there is an increasing demand for longevity connected to an increasing use in a younger population, more active lifestyles in the patient group and high life expectancy. The failures in the short term (<3 years) are often related to fracture, dislocation or infection, whereas in the long term (>5 years) osteolysis and loosening are the most common reasons for revision [1–4].

Implant design and material combinations have a strong effect on the outcome [1–4]. A common material couple in hip joint replacements is a metal femoral head with an ultra-high molecular weight polyethylene (UHMWPE) cup. The wear debris of UHMWPE has been linked to osteolysis and implant loosening [5]. However, a younger generation of the highly cross-linked UHMWPE (HXLPE) has shown similar type of wear debris but lower wear rates, thereby reducing the negative biological response [6,7]. The clinical results so far are promising [1,3,4]. Alternatively, for cobalt chromium molybdenum alloys (CoCrMo), commonly used in joint replacements, failure modes are linked to the corrosion products and metal ions, especially when coupled with another CoCrMo surface, where hypersensitivity, metallosis and pseudotumours have been reported [8,9]. For ceramic materials, commonly zirconia-toughened alumina, failures have been linked to their mechanical properties. Reported limitations have included fractures related to the brittle behaviour, chipping on insertion and mal-positioning, and squeaking due to stick–slip phenomena [10].

Silicon nitride materials were introduced to orthopaedics less than 10 years ago [11], and the first silicon nitride femoral head was implanted 2011 [12]. Advantages of silicon nitride are mainly its high wear resistance [13], its ability to slowly dissolve in aqueous solutions [14–16], its biocompatibility and bacteriostatic properties [17–21]. The ability of silicon nitride wear debris to dissolve in aqueous environments may potentially limit any negative biological reactions and thus increase the longevity of the implants. As an alternative to bulk silicon nitride, this study considers silicon nitride (SiN_x) coatings [22–24] that possess the above-mentioned potential advantages. Moreover, SiN_x coatings on a metal offer a possibility to retain the benefit of a ductile bulk material and possibly avoid the risk of catastrophic fracture, which has been a concern for ceramics.

Ideally, the dissolution rate should be a compromise between a relatively quick dissolution of the wear debris and a long-lasting coating. A high dissolution rate of the wear debris may reduce the risk of negative biological reactions or third body abrasion, whereas the coating service life is enhanced by a slow dissolution rate. Additionally, the coatings are believed to act as a barrier and reduce metal ion release.

* Corresponding author.
E-mail address: cecilia.persson@angstrom.uu.se (C. Persson).

http://dx.doi.org/10.1016/j.msec.2016.01.049

These coatings could potentially be employed in tribological contacts, such as on joint bearing surfaces and modular taper junctions. While CoCrMo is commonly used for joint bearing surfaces such as hip heads, titanium based alloys are commonly used where wear resistance is not decisive and osseointegration is a priority, e.g. in the femoral stem. Taking into consideration also the health concerns related to ion and particle release from CoCrMo alloys in malfunctioning prostheses, CoCrMo was chosen as substrate as well as control material for the current study.

The main aim of this study was to quantify the dissolution rate of SiN_x coatings. This was done as a function of the N/Si ratio, which has previously been shown to affect the mechanical properties of the coatings [25]. A second aim of the study was to evaluate whether SiN_x coatings deposited on CoCrMo could reduce the release of metal ions into the surroundings. The coatings were tested in a static environment, without any mechanical loading, and compared to CoCrMo.

2. Materials and methods

Custom-made holders were produced to study the materials in contact with simulated body fluid over 60 days. Electrochemical monitoring was applied throughout the test, and solution and surface analysis were performed upon test completion.

2.1. Materials and test solution

Four types of SiN_x coatings were deposited by reactive high power impulse magnetron sputtering (HiPIMS, CemeCon CC800/9 ML, Germany) on CoCrMo substrates, polished to a roughness of 11 ± 2 nm. The deposition parameters are displayed in Table 1. The coating thickness ranged between 7.0 to 7.5 μm. One type of coating, referred to as a standard coating, was based on the deposition parameters from previously investigated SiN(1/−/l) (deposited at 1 kW with a 'low' deposition temperature of 110 °C) [23]. These dense coatings typically contain low amounts of oxygen and argon (<5 at.%), are x-ray amorphous and display only a short range ordering in TEM [23]. This standard coating, $SiN_{0.8(std)}$, was evaluated for time dependence and thus stopped at dissolution durations of 3, 11, 30 and 60 days. For these measurements two coated samples per time point were assessed. Three more coatings with different nitrogen contents referred to as $SiN_{0.3}$, $Si_{0.8}$, and $SiN_{1.1}$, were considered for the entire time range of 60 days. Here, one sample per coating type was measured. Two uncoated CoCrMo samples served as the reference material. The reference and substrate (upon which the coatings were deposited) material was low carbon wrought CoCrMo (ASTM F 1537, Peter Brehm, Germany) with the following composition in wt.%: Co (bal.), Cr (26–30), Mo (5–7), Ni (<1), Si (<1), Mg (<1), Fe(<0.75), N (<0.25) and C (<0.14). The average surface roughness prior to testing was determined using vertical scanning interferometry (VSI, Wyko NT-1100, Vecco, USA) and a 10× objective evaluating an area of 450 μm by 590 μm. Five samples, with five areas per sample, were evaluated for surface roughness and are summarized in Table 1.

Each sample was placed at the bottom of a custom made polyoximethylene holder and connected as working electrode (WE) as shown in Fig. 1, and incubated in a 37 °C oven for the test duration. Three separate wells were created on each sample (see Fig. 1a), each with a diameter of 8 mm and a height of 80 mm. Each well was filled with 4 ml of a simulated body fluid. The fluid was made from 25 vol.% foetal bovine serum solution (FBS, Sera Laboratories International Ltd., West Sussex, UK), diluted in a phosphate buffered saline solution (PBS, Sigma-Aldrich, Co., St. Louis, USA) and 0.03 vol.% sodium azide (GBioscienics, St. Louis, USA). The solution was extracted from the wells every week, and refilled with fresh solution after triple rinsing with deionized water. The solution had an initial pH between 7.4 and 7.7, and was stored at −20 °C before and after testing. In order to avoid metal contamination, any handling of the solutions was done with polymeric utensils.

The customized holder was developed to permit simultaneous dissolution rate measurements at several points for discs coated on one side and to hold a fluid volume similar to the natural joint [26–28]. The setup proportion between the surface area and solution however does not reflect a full hip prosthesis, as the surface area in the setup was 50 mm^2, whereas a sphere with 28 mm in diameter, resembling a femoral head, has a surface area of approximately 2500 mm^2. The same liquid to surface area ratio corresponds to 200 ml fluid to a femoral head. The relatively small area that was used reduces the risk of saturating the solution and enables testing in an earlier stage of material development. In a hypothetically fully static hip more ions would be released due to the larger area. However, the dissolution rate and general trend for the different materials is expected to be assessable in relation to each other.

2.2. Corrosion assessment

On the top of each well a folded 100 mm long platinum wire was connected as a counter electrode (CE, PT-02, Web Scientific Ltd. Crewe, UK). An Ag/AgCl reference electrode (RE) was assembled from the top (RE-4, MW-2021, BASi Inc. IN, USA). Each interface between sample, holder, and well was sealed by a rubber gasket. The open circuit potential (OCP) and linear polarisation scans (LPR) were recorded at least three times per week by connecting each well to a potentiostat (PGSTAT101, Metrohm Autolab B.V., Utrecht, Netherlands). LPR were recorded in the range of ±20 mV from the OCP, using a step width of 1 mV at a speed of 1 mV/s. The LPR measurements were used to calculate the resistance to polarisation and the corrosion current according to Stern-Geary [29]. For the CoCrMo reference sample a Tafel constant of 120 mV/decade was assumed [30]. The anodic and cathodic Tafel constants for $SiN_{0.8(std)}$ were determined from polarisation scans as shown in Fig. 2. Therefore, $\beta_a = +221$ mV/decade and $\beta_c = -269$ mV/decade was assumed for all SiN_x coatings. The corrosion current was used to estimate the anodic mass loss from oxidation by Faradays law. The half-cell reactions assumed in the calculation were: $Co \rightarrow Co^{2+} + 2e^-$ ($Z = 2$) for CoCrMo [31] and $Si \rightarrow Si^{4+} + 4e^-$ ($Z = 4$) for SiN_x coatings. This, in turn, presumes that no current contribution from other reactions, no change of state, or other reactions in the solution contributes to the current. The total charge was obtained by integration of the corrosion current over the time. The dissolution rate was calculated in nm/day from the corrosion current (I_{corr}), assuming a density of 9.15 g/cm^3 for CoCrMo [32], 3.2 g/cm^3 for SiN_x coatings [33], and general homogeneous dissolution across the exposed area. In order to estimate the volume loss of SiN_x coatings, only dissolution of Si was assumed to contribute to the corrosion current. Moreover, the

Table 1
Deposition parameters for the four types of SiN_x coatings investigated with the composition of Si and N in the coating obtained by XPS, and the average surface roughness evaluated by VSI.

Name	Substrate temperature [°C]	Si target power [kW]	Pulse frequency [Hz]	Negative bias voltage [V]	N_2/Ar flow ratio	N/Si atomic ratio in coating	Average surface roughness (R_a), [nm]
$SiN_{0.8(std)}$	350	1	300	100	0.17	0.77	17 (±3)
$SiN_{0.3}$	200	0.6	200	100	0.06	0.34	13 (±2)
$SiN_{0.8}$	200	0.6	200	100	0.17	0.79	11 (±2)
$SiN_{1.1}$	200	0.6	200	100	0.31	1.12	13 (±3)

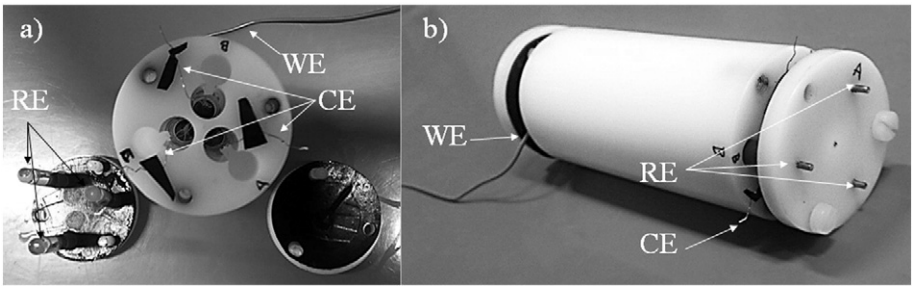

Fig. 1. Top view a) and side view b) of an assembled holder without solution with working electrode (WE), reference electrode (RE) and counter electrode (CE).

volume of N in the SiN_x structure was accounted for, by a volume increase of 15% for $SiN_{0.3}$, 40% for $SiN_{0.8}$ and 55% for $SiN_{1.1}$.

2.3. Solution analysis

Inductively coupled plasma mass spectrometry (ICP-MS, NexION 300d, PerkinElmer, USA) was applied to determine the ion concentration of Co, Cr, and Mo in the solution. Here, the isotopes of Co-59, Cr-52, and Mo-98 were evaluated and In was used as internal standard element. Prior to ICP analysis 0.5 ml of defrosted solutions was diluted 1:10 with deionized water. Results from blank solution measurements were subtracted from the test results to determine a zero concentration at day 0. One time point per week was analysed for the first three weeks of the experiment. The cumulated ion concentration was calculated in μg per well. For each sample of CoCrMo, $SiN_{0.3}$ and $SiN_{1.1}$, two wells were analysed. The material densities stated above were used to calculate the dissolution rate in nm/day.

2.4. Surface analysis

The dissolution depth, as derived from the step height on the edge of the dissolution area, was determined using vertical scanning interferometry (VSI, Wyko NT-1100, Vecco, USA) with a 2.5× objective from one cleaned dissolution area per sample. The step height was determined by evaluating 18 lines per sample, with a width of 50 μm and a length of ~500 μm, applied 90° to the edge of dissolution. Surface appearance and chemistry with a lateral resolution and depth information in the sub-μm range were evaluated using a field-emission gun scanning electron microscope (FEG-SEM), with in-lens detector and secondary electron detector at 10 kV (Merlin, Carl Zeiss Microscopy GmbH, Germany), with integrated energy-dispersive x-ray spectroscopy (EDS, X-Max 80 mm^2, and Aztec software).

The chemical bonding and composition on the outermost nm's was examined using x-ray photoelectron spectroscopy (XPS, Physical Electronics (Phi) Quantum 2000, USA). In order to investigate the chemistry of the bulk, measurements were taken after 10 min sputter cleaning at 1 keV. Core level spectra were analysed using the software XPS Peak after Shirley-type background correction using Gaussian fits for Si2p core level spectra, without further restrictions. The N/Si atomic ratio of SiN_x coatings stated in Table 1 was determined using another XPS instrument (Axis Ultra DLD, Kratos Analytical, Manchester, UK). The ratios were obtained from measurements after 2 min sputter cleaning at 2 keV. After subtraction of a Shirley background the compositions were extracted using elemental cross sections provided by Kratos Analytical. Both XPS instruments used a monochromatic Al–Kα source, Ar^+ ions for sputter cleaning and automatic charge compensation throughout the acquisition.

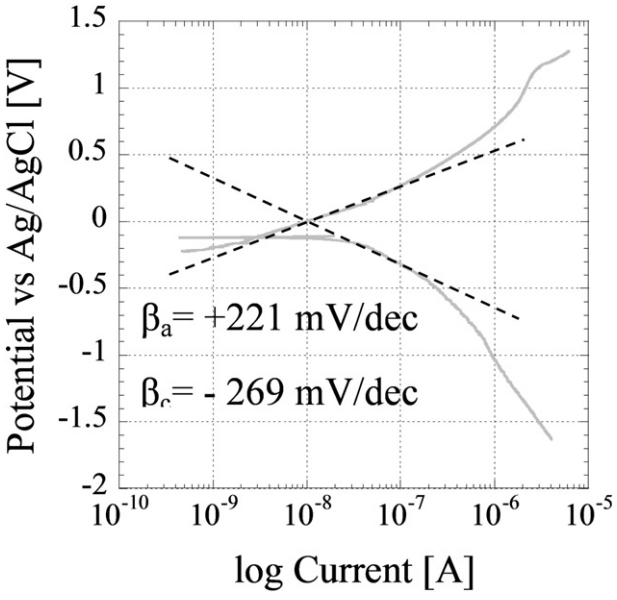

Fig. 2. Anodic and cathodic polarisation scans for $SiN_{0.8(std)}$ for determination of Tafel constants $\beta_a = +221$ mV/decade and $\beta_c = -269$ mV/decade, used for calculation of corrosion current for the SiN_x coatings.

3. Results

3.1. Electrochemical evaluation

Upon immersion of CoCrMo, the OCP started at −0.3 V and slowly ennobled for the first day as seen in Fig. 3. After the first week of immersion, variations between 0 and −0.7 V were observed until day 60. The OCP of $SiN_{0.8(std)}$ started at −0.2 V and decreased during the first days. The OCPs for $SiN_{0.3}$ and $SiN_{0.8}$ were comparable to $SiN_{0.8(std)}$ with potentials varying between −0.2 to −0.8 V, and were generally lower than CoCrMo. $SiN_{1.1}$ showed comparatively high potential levels, similar to CoCrMo, fluctuating between 0 to −0.7 V. The median and mean OCPs over 60 days are summarized in Table 2. The median OCP for CoCr and $SiN_{1.1}$ were more noble (−0.22 to −0.28 V) than the other SiN_x coatings (−0.38 to −0.51 V).

The corrosion current (I_{corr}) (presented as median and mean values in Table 2) was overall stable for 60 days, with the exception of both CoCrMo samples, which showed a one order of magnitude increase in the corrosion current at days 17, 18 and 34. $SiN_{0.8(std)}$ and $SiN_{0.8}$ showed similar corrosion currents of around 9 nA. For $SiN_{0.3}$ the corrosion current increased to a median of 25 nA, while the $SiN_{1.1}$ remained at approximately 2 nA.

As shown in Fig. 4, the total charge (Q_{tot}) passing through CoCrMo samples was 0.40 and 0.46 C after 60 days. CoCrMo samples showed a higher total charge than SiN_x coatings. Over the course of 60 days the Q_{tot} of the SiN coatings increased to values of 0.02 and 0.28 C. As a consequence of the peaks in corrosion current, escalations in the total charge were observed for CoCrMo and $SiN_{0.3}$. Disregarding these step increases, an approximately linear increment of the total charge was seen for all samples. The total charge was highest for CoCrMo, followed by $SiN_{0.3}$, then $SiN_{0.8(std)}$ and $SiN_{0.8}$ at a similar total charge and finally $SiN_{1.1}$. The latter showed half the total charge of $SiN_{0.8(std)}$ and $SiN_{0.8}$.

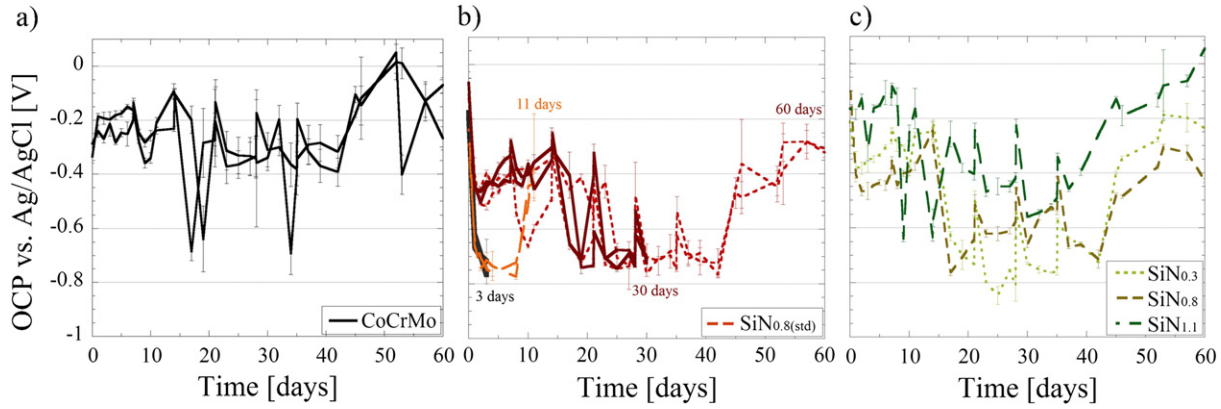

Fig. 3. OCP ± standard deviation per sample, related to a Ag/AgCl reference electrode for a) CoCrMo, b) $SiN_{0.8(std)}$ for 3, 11, 30 and 60 days and c) $SiN_{0.3}$, $SiN_{0.8}$, and $SiN_{1.1}$.

The median and mean increase of the total charge per day (Q) is shown in Table 2.

The estimated dissolution rate, expressed as nm/day, is shown in Fig. 5. The dissolution rates extracted from electrochemical measurements are labelled I_{corr}. For the $SiN_{0.8(std)}$ the dissolution rate increased during the first days starting from 0.2 nm/day to later plateauing around 0.6 nm/day. The peak values of the corrosion current observed for CoCrMo and $SiN_{0.3}$ affected the calculated dissolution rate. When including these peak values for CoCrMo, a rate of 4.6 and 5.1 nm/day was obtained over the course of 60 days (not shown in the figure). If the dissolution rate instead was calculated from the first days (without peaks in the current) the dissolution rates were 0.7 nm/day and 0.8 nm/day. For $SiN_{0.3}$, the dissolution rates were estimated to 2.4 nm/day (including corrosion current peaks) or 0.4 nm/day (excluding corrosion current peaks). The lowest dissolution rate calculated from the corrosion current was for $SiN_{1.1}$ at 0.2 nm/day.

3.2. Solution analysis

The ion concentration in the solution of Co, Cr, and Mo is shown in Fig. 6. The cumulated ion concentration of Co, Cr, and Mo in the solution was one to two orders of magnitude higher for CoCrMo compared to the SiN_x coated samples. For CoCrMo samples, the relative ion concentration of Co, Cr, and Mo in the solution was 66, 27, and 7 wt.%, respectively, after three weeks. This corresponds to a total Co, Cr and Mo weight of 10 to 11 μg, while $SiN_{0.3}$ and $SiN_{1.1}$ had losses of 0.1 to 0.2 μg, respectively. The dissolution rate calculated from ICP measurements for CoCrMo was 1.1 and 1.2 nm/day (Fig. 5b).

3.3. Surface analysis

The dissolution depth determined by VSI is summarized in Table 3. An increased dissolution depth with time was observed. The dissolution depth at day 3 was found to be below the detection limit of VSI measurements. The edge of the dissolution area is exemplified for $SiN_{0.8(std)}$, CoCrMo, $SiN_{0.3}$, $SiN_{0.8}$, and $SiN_{1.1}$ in Fig. 7. The dissolution rate obtained by VSI measurements was 1.1 to 1.4 nm/day for $SiN_{0.8(std)}$ and 1.0 nm/day for CoCrMo, shown in Fig. 5. The dissolution depth was lowest for $SiN_{1.1}$, with an estimated dissolution rate of 0.4 nm/day.

Table 2
Median and mean OCP, I_{corr} and Q per day evaluated over 60 days of SiN_x coatings and CoCrMo.

Name	OCP [V] median (mean)	Average I_{corr} [nA] median (mean)	Q per day [mC] median (mean)
$SiN_{0.3}$	−0.38 (−0.48)	25 (47)	2.0 (2.5)
$SiN_{0.8(std)}$	−0.44 (−0.50)	10 (10)	0.6 (0.7)
	−0.51 (−0.53)	9 (10)	0.7 (0.7)
$SiN_{0.8}$	−0.46 (−0.48)	8 (9)	0.7 (0.7)
$SiN_{1.1}$	−0.26 (−0.29)	2 (4)	0.3 (0.3)
CoCrMo	−0.28 (−0.27)	16 (82)	5.1 (5.5)
	−0.22 (−0.24)	12 (55)	5.0 (5.6)

In the dissolution area, a layer from the solution had formed on the coatings observed by SEM in Fig. 8. The layer did not homogeneously cover the surface, but for the specific adsorbed regions, EDS mapping revealed an elemental increase of C, and O (dark in the SEM), and in elements resulting from the solution such as crystals of Na and Cl (larger, bright in SEM), as well as P and Ca (smaller, bright in SEM). A cleaned dissolution area was not possible to differentiate from an original coating surface, i.e. no local dissolution variations were observed.

XPS measurements were performed outside the dissolution area prior and post Ar^+ sputter cleaning providing information from the surface, and the bulk coating (SiN_x) or bulk metal (CoCrMo). These areas will be denoted '*surface*' and '*bulk*', respectively. The corresponding XPS results are shown in Figs. 9 and 10. Measurements inside the dissolution area were carried out on the surface layer after testing, denoted '*layer*', and after cleaning by rubbing with an ethanol tissue denoted '*dissolution*' area.

The *bulk* CoCrMo (measured after sputter clean) XPS survey spectrum, Fig. 9, contains signals from Co, Cr, Mo, and Fe. The corresponding core level spectra of Co2p, Cr2p, and Mo3d (Mo3d not shown in figure) comprise mainly signals from metallic Co, Cr and Mo bonds. On the *surface* (prior to sputter cleaning) the survey spectrum of the CoCrMo shows signals from C, O, Co, Cr, and Fe. The corresponding Cr2p and Co2p core level spectra comprise contributions assigned to Co and Cr bond to O and C. The Cr2p core level spectra from the *surface*, and less intense of the *dissolution* area showed a peak at ~576.8 eV, assigned to either Cr_2O_3 and/or $Cr(OH)_3$ [34,35]. In addition, the Co2p core level spectra from the *surface* showed a peak assigned to metallic Co bonds. The survey spectrum obtained from the *dissolution* area showed a presence of O, Cr, C, N, Na, Ca, and traces of Mg and P, where Na, Ca, Mg, and P originated from the PBS. In the survey spectra in Figs. 9 and 11 of the *layer* that adsorbed from the solution on the dissolution area, C, N, and O were found for both CoCrMo and all SiN_x coatings.

The survey spectrum of the *bulk* SiN_x coatings showed signals from Si, N and Ar, exemplified by $SiN_{0.8(std)}$ in Fig. 10. The *surface* and *dissolution* area contained signals from O, C, Si, N, and Ar. Additionally, Ca was detected in the *dissolution* area. The core level spectra of Si2p revealed differences between the SiN_x coatings. Peak fitting of SiN_x coatings showed three main contributions at ~103.9 eV, ~101.4 eV, and ~99.9 eV, assigned to Si–O, Si–N, and Si–Si bonds, respectively [36–39]. With few bonded N atoms the Si–N peak shifts towards lower binding energies ~100.1 eV [40].

The *bulk* core level spectra for $SiN_{0.8(std)}$ comprised two peaks; at 101.5 eV assigned to Si–N bonds, and at 99.8 eV assigned to Si–Si

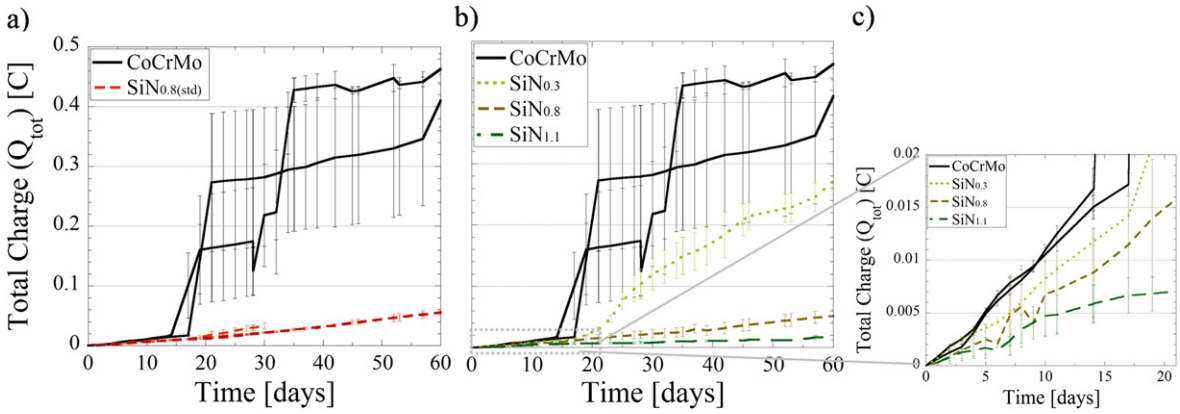

Fig. 4. Total charge going through the working electrode ± standard deviation between the wells per sample for CoCrMo and a) $SiN_{0.8(std)}$ for 3, 11, 30 and 60 days and b–c) for $SiN_{0.3}$, $SiN_{0.8}$, and $SiN_{1.1}$.

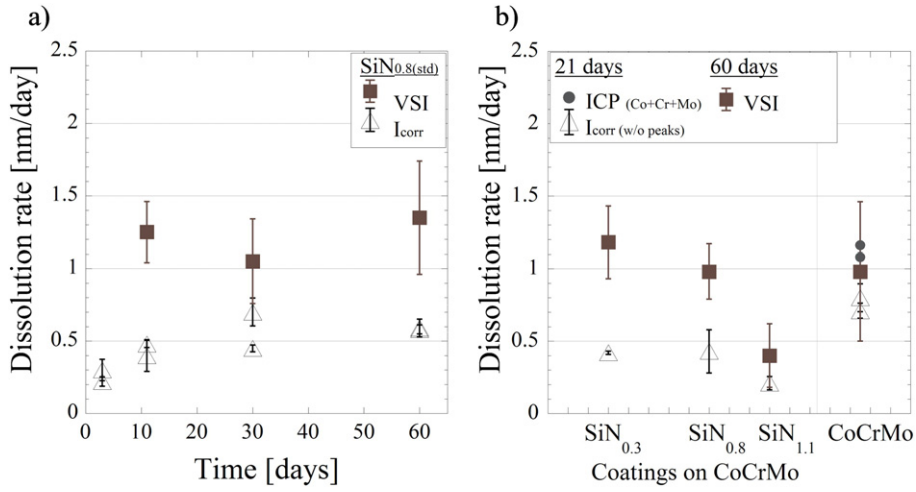

Fig. 5. Comparison of dissolution rates obtained from electrochemical measurements of I_{corr}, the step height measured using VSI, and from the ion concentration in the solution measured with ICP. In a) the dissolution rate of $SiN_{0.8(std)}$ over time is shown, in b) the dissolution rate of $SiN_{0.3}$, $SiN_{0.8}$, and $SiN_{1.1}$ based on measurements from 21 or 60 days.

bonds. On the *surface* and in the *dissolution* area a third peak can be distinguished at ~103.9 eV, assigned to Si–O bonds [41]. The bonding structure for $SiN_{0.8}$ was the same as $SiN_{0.8(std)}$; for the *bulk* a distinct peak at 101.7–101.9 eV (Si–N) was observed, and a less intense contribution at 100.1–100.2 eV (Si–Si). For the *surface* and in the *dissolution* area a third peak at 103.7 eV (Si–O) was observed.

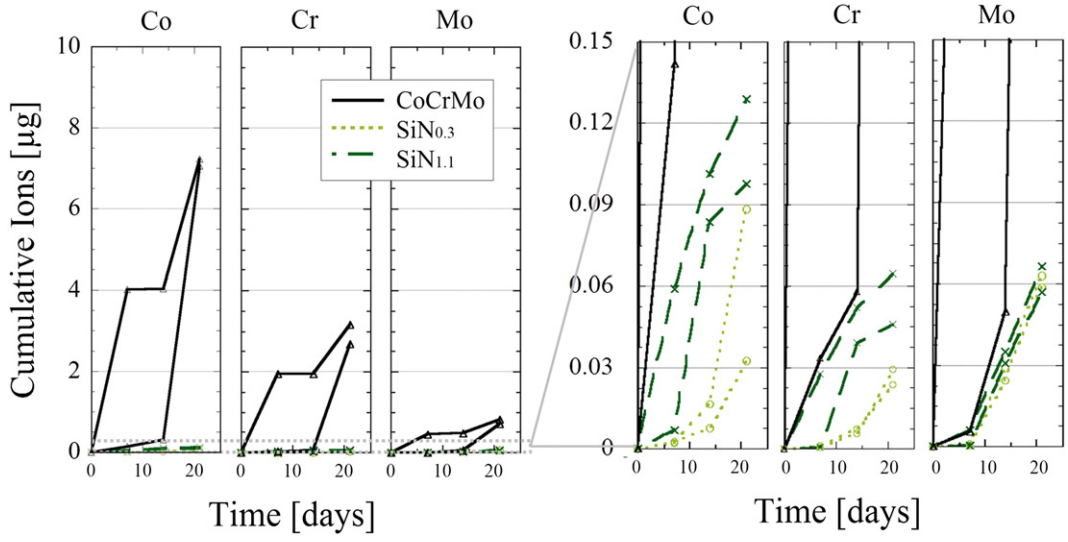

Fig. 6. Ion content (Co, Cr and Mo) of the solutions in contact with CoCrMo, $SiN_{0.3}$ or $SiN_{1.1}$, for the first three weeks of testing. Two separate wells per sample were used and the ion content was measured with ICP. Lower concentrations can be observed in the enlargement to the right.

Table 3
Dissolution depth ± standard deviation obtained using VSI on the edge of the dissolution area (18 steps around one dissolution area).

	$SiN_{0.8(std)}$				CoCrMo	$SiN_{0.3}$	$SiN_{0.8}$	$SiN_{1.1}$
[Days]	3	11	30	60	60	60	60	60
[nm]	–	17 ± 3	31 ± 9	81 ± 23	59 ± 29	71 ± 15	59 ± 11	24 ± 13

The *bulk* core level spectra from the $SiN_{0.3}$ coating showed two contributions; a dominant peak at 99.6 eV assigned to Si–Si and a contribution at 100.4 eV assigned to Si–N bonds. On the *surface* and in the *dissolution* area a peak at ~104 eV appeared, which was assigned to Si–O. The Si2p core level from the *bulk*, the *surface* and the *dissolution* area of $SiN_{1.1}$ showed a Si–N peak (~100.5–101.0 eV). The Si2p core level of the *dissolution* area obtained from $SiN_{1.1}$ did not show any clear evidence of Si–O bonds.

4. Discussion

Based on the results of this study, the chemical components, structures and ions resulting from the two systems of SiN_x coatings and CoCrMo in contact with ambient air and the simulated body fluid, are schematically illustrated in Fig. 11. This study has demonstrated that SiN_x coatings deposited by HiPIMS could be an effective method to reduce the release of corrosion products from CoCrMo in a static environment of simulated body fluid.

4.1. Electrochemistry and dissolution

The dissolution properties of $SiN_{0.8(std)}$ and $SiN_{0.8}$ were not notably affected by the differences in HiPIMS deposition parameters (substrate temperatures, average target power and pulse frequency). An effect on the dissolution rate was however found for the different N/Si ratios in the coatings. The dissolution rate calculated from the corrosion current and VSI showed decreasing values for increasing N/Si atomic ratios. This may be related to increased amounts of comparatively strong Si–N bonds and suggests that the dissolution rate of SiN_x can, to some extent, be tuned by the N content in the coating. For a SiN_x coating with a thickness of 7.5 μm, as in this study, and a dissolution rate of 0.4 nm/day ($SiN_{1.1}$), 50 years would be needed to dissolve the coating entirely in a non-contact static situation. This corresponds to approximately 2 atomic layers per day. The dissolution rate of SiN_x coatings was similar to what has been found in vivo for silicon nitride coatings produced by chemical vapour deposition (CVD), which showed dissolution rates between 0.33 to 2.0 nm/day in mice [42], and 0.2 μm lasted more than a year implanted in a guinea pig (<0.56 nm/day) [43]. The dissolution rate of silicon nitride is higher for strong bases and increased temperatures [14,15]. Further evaluations using different pH, as well as studies considering the interactions between wear and corrosion are encouraged, as the pH may vary and be acidic for an infected hip [44].

For CoCrMo a fair agreement was found between the dissolution rates estimated from the corrosion current excluding the peak currents, VSI and ICP (0.7 to 1.2 nm/day). If the peaks in current were included a rate of around 5 nm/day was obtained. Other electrochemical evaluations in the literature for wrought CoCrMo in different FBS

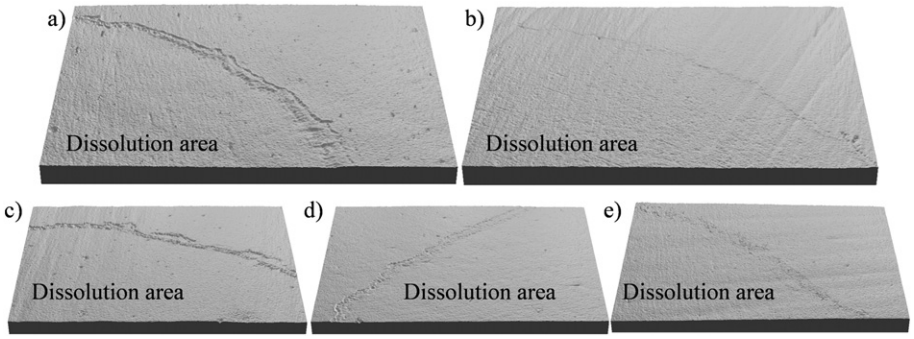

Fig. 7. 3D VSI plots displaying the edge of the dissolution area illustrating the dissolution depth for a) $SiN_{0.8(std)}$ and b) CoCrMo, c) $SiN_{0.3}$, d) $SiN_{0.8}$, and e) $SiN_{1.1}$ after 60 days. The area plotted is 1800 × 2400 μm, the height if the base is approximately 1 μm and is amplified in order to visualize the steps.

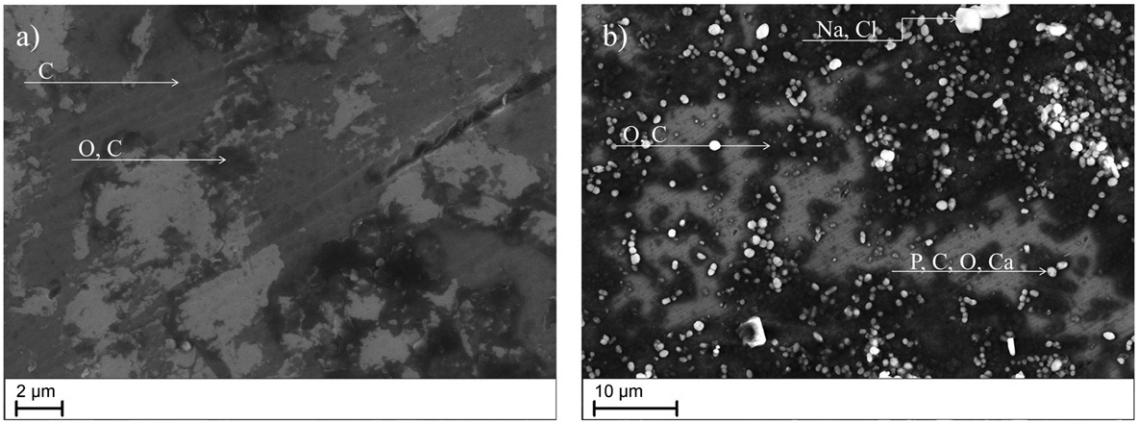

Fig. 8. SEM images of $SiN_{0.3}$, after 60 days of dissolution, showing a layer of O and C on the coating, which is still visible underneath. In some regions particles containing Ca, Na, Cl, and P had formed as shown in b).

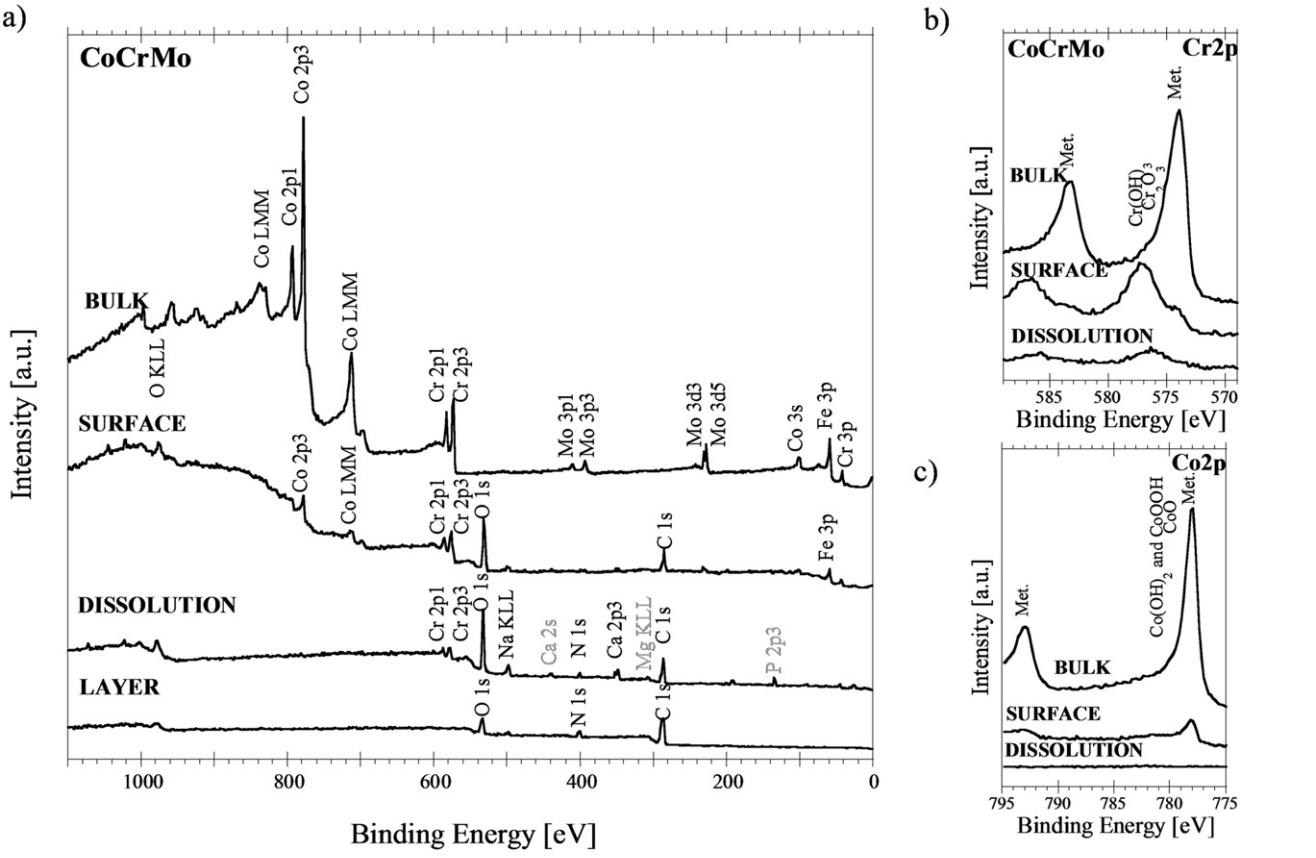

Fig. 9. XPS spectra for CoCrMo in the bulk (after sputtering), on the surface (without contact with the solution), in the dissolution area (after cleaning and removal of the layer built up from the solution) and on the outermost layer (formed from the solution), in a) as survey scans and in b) and c) core level spectra for Cr2p and Co2p.

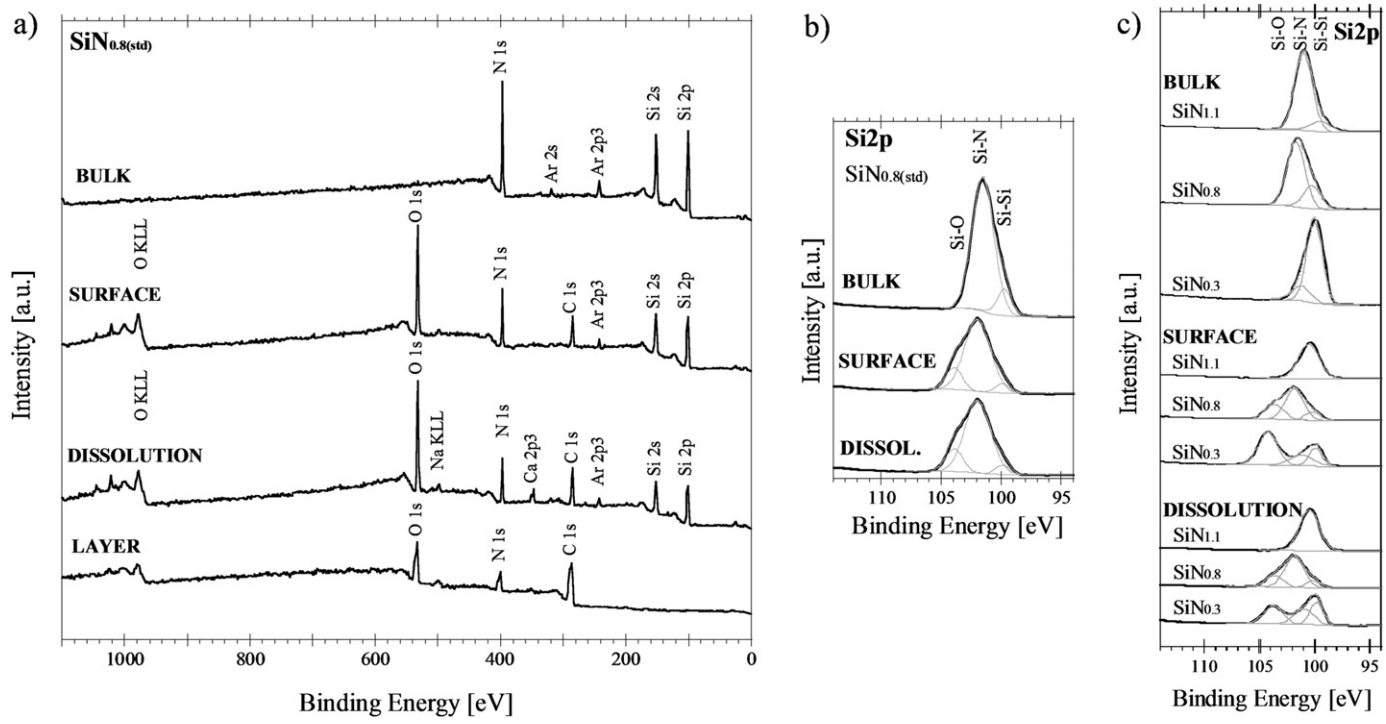

Fig. 10. XPS spectra for SiN_x coatings in the bulk coating (after sputtering), on the surface (without contact with the solution), and in the dissolution area (after cleaning and removal of outer layer) and on the outermost layer (formed from the solution), in a) as survey scan for $SiN_{0.8(std)}$ and Si2p core level spectra for $SiN_{0.8(std)}$ in b) and $SiN_{0.3}$, $SiN_{0.8}$, and $SiN_{1.1}$ in c).

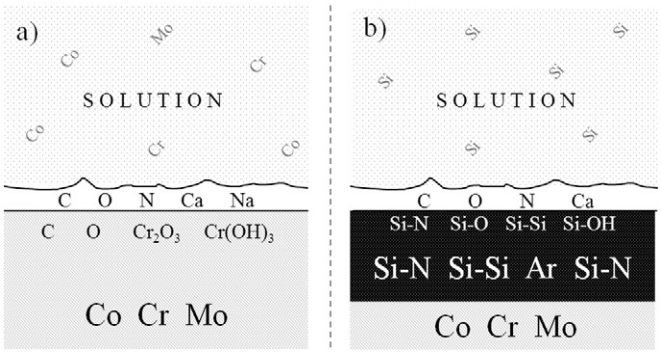

Fig. 11. Schematic sketch over bulk, surface and solution elements, ions, bonds and structures seen in this study in a) CoCrMo and in b) $SiN_{0.8(std)}$ coating on CoCrMo substrate.

concentrations in PBS report dissolution rates between 1 and 10 nm/day [45], while a study on Co–20Cr–15W–10Ni (ASTM F-90) in Ringer's solution showed a corrosion rate of 0.8 nm/day [46]. The wide range of dissolution rates found in the literature covers the full range seen in this study. As ICP-MS and VSI techniques showed a dissolution rate closer to the results calculated without the current peaks, it was argued that the data excluding the peaks is a closer approximation. Deviations could arise due to measurement error or assumptions connected to the Tafel constants. Several assumptions were made for the estimation of the ionic mass loss from the corrosion current under static conditions; the specific dissolution reactions of Co and Si, Tafel constants, also it is assumed that no other reactions in the solution affected the current. The effect of different Tafel constants on the dissolution rate is assessed in the supplementary information. Nevertheless, dissolution rates extracted from ICP and VSI measurements showed similar values and trends compared to those calculated from the corrosion current when excluding the singularities in the corrosion current (Fig. 5). Although the results are of the same order of magnitude, the dissolution rates determined from the corrosion current for SiN_x coatings were approximately half of what was obtained from VSI. The difference may be related to the assumptions made for the electrochemical calculations mentioned above, or for the VSI a potential overestimation may stem from inhomogeneous dissolution, as only a few hundreds of μm's were considered. However, no indication of inhomogeneous dissolution was observed.

The open circuit potential and corrosion current after one to two weeks showed an increasingly irregular behaviour. The current peaks may be induced by local, shorter corrosion events, such as pitting, or (for CoCrMo) intergranular corrosion. However, VSI and SEM provided no evidence for this. As the recording frequency was relatively low, it is reasonable to assume that shorter corrosion events may have occurred between measurements that were not observed in the corrosion current. ICP including the first three weeks, and especially VSI, including the full 60 days, should include the effect that these peaks may have had on the corrosion rate.

4.2. Surface and reactions

Inside the dissolution area the dissolution appeared homogenous in VSI and SEM, e.g. no localized dissolution around defects could be distinguished. The adsorbed layer from the solution, seen in SEM in Fig. 8, did not show full coverage on the surface, although it was observed for all coatings and to a higher extent on CoCrMo samples. Even though chromium oxide/hydroxide on the CoCrMo surface could reduce the dissolution rate [34,35,47], the ion measurements showed a ratio between Co, Cr, and Mo ions (66/22/7 wt.%) that was similar to bulk CoCrMo (58–69/26–30/5–7 wt.%) during the first three weeks. The presence of albumin in PBS has previously been found to increase the corrosion rate of CoCrMo [48].

The bonding structure for SiN_x coatings showed a distinct signal from Si–N bonding in the *bulk* for all coatings except the low nitrogen coating $SiN_{0.3}$ where the distinct peak at lower bonding energy on the Si2p core level spectra was assigned to Si–Si bonds, possibly also affected by N as a neighbour. On the surface and in the dissolution area Si–O bond formation was observed for the coatings especially when N/Si < 1.1. The bonding structure supports the chemical reaction associated with dissolution of silicon nitride in water and in a tribological contact, i.e. $Si_3N_4 + 6H_2O \rightarrow 2SiO_2 + 4NH_3$ and $SiO_2 + 2H_2O \rightarrow Si(OH)_4$ [14,15,49], even though the results do not clearly show the presence of $Si(OH)_4$. Further studies to understand if and to what extent ammonia forms would be of interest. A low concentration of ammonia can naturally form in the body and is processed by the kidney and the liver, however elevated levels of ammonia can be an issue [50]. The higher nitrogen-containing coating (N/Si ≥ 1.1) did not show any evident Si–O bonds on the surface or in the dissolution area, which was most likely related to the stable Si–N bond with a higher binding energy than Si–Si and a higher degree of fully terminated Si–N surface [51].

In this study, the static dissolution of SiN_x coatings and CoCrMo was investigated. It should be noted that if a solution flow or wear would be introduced the mechanisms of mass loss may differ substantially through introduction of e.g. surface oxide removal, disturbances in corrosion mechanisms, presence of wear debris etc. and the present results can only be related to static dissolution conditions. The low number of samples used per group can be considered a limitation to the study. However, the combined values, of e.g. dissolution rates, correlated well with literature, and trends in terms of nitrogen content in relation to dissolution rate corresponded well with trends in chemical bonding.

5. Conclusions

The dissolution of SiN_x coatings in simulated body fluid containing FBS and PBS was investigated over 60 days and compared to CoCrMo. This study illustrated the importance of combining electrochemical measurements with other methods to calculate the dissolution rate in order to be able to fully interpret the results. The following conclusions can be made:

Differences in behaviour between SiN_x coatings and CoCrMo alloy:

- Overall the SiN_x coatings showed a lower OCP, a lower and more stable corrosion current, and a lower oxidation mass loss than CoCrMo.
- SiN_x coatings on CoCrMo reduced the release of metal ions into the solution by two orders of magnitude.
- CoCrMo showed a dissolution rate between 0.7 and 1.2 nm/day, while the SiN_x coatings showed dissolution rates between 0.2 and 1.2 nm/day.

Effect of nitrogen content in the coating:

- Increased nitrogen contents in the coating resulted in reduced dissolution rates, down to 0.2 and 0.4 nm/day.
- The highest nitrogen containing coating ($SiN_{1.1}$), showed mainly Si–N bonds in the bulk, at the surface and in the dissolution area.
- The lower nitrogen containing coatings ($SiN_{0.3}$ and $SiN_{0.8}$) showed Si–N and/or Si–Si bonds in the bulk, and an increased formation of Si–O bonds at the surface as well as in the dissolution area.

Effect of time, for SiN_x coatings as well as CoCrMo:

- After initial stabilization for the first two weeks the electrochemical system (OCP and I_{corr}) entered a more fluctuating behaviour until day 60.
- A nearly linear increase in mass loss with time (ionic and calculated from I_{corr}) was observed for the first 60 days.

Acknowledgements

The research leading to these results has received funding from the European Union's Seventh Framework Programme (FP7/2007–2013) under the LifeLongJoints Project, Grant Agreement no. GA-310477. Dr.

Schmidt acknowledges the support by the Carl Tryggers Foundation for Scientific Research (CTS 14:431). The authors would also like to acknowledge Jean Pettersson for input and help with the ICP measurements and Peter Brehm GmbH for supplying the cobalt chromium alloy.

Appendix A. Supplementary data

Supplementary data to this article can be found online at http://dx.doi.org/10.1016/j.msec.2016.01.049.

References

[1] Swedish hip arthroplasty register, Annual report, 2013.
[2] National joint registry for England, Wales and Northern Ireland, Annual Report, 2014.
[3] The New Zealand joint registry, Annual Report, 2014.
[4] Australian orthopaedic association's national joint replacement registry, Annual Report, 2014.
[5] E. Ingham, J. Fisher, The role of macrophages in osteolysis of total joint replacement, Biomaterials 26 (11) (2005) 1271–1286.
[6] A.L. Galvin, J.L. Tipper, L.M. Jennings, M.H. Stone, Z.M. Jin, E. Ingham, et al., Wear and biological activity of highly crosslinked polyethylene in the hip under low serum protein concentrations, Proc. Inst. Mech. Eng. H J. Eng. Med. 221 (1) (January 1, 2007) 1–10.
[7] R.M. Baxter, D.W. MacDonald, S.M. Kurtz, M.J. Steinbeck, Characteristics of highly cross-linked polyethylene wear debris in vivo, J. Biomed. Mater. Res. B Appl. Biomater. 101 (3) (2013) 467–475, http://dx.doi.org/10.1002/jbm.b.32902 (Epub 2013 Feb 22).
[8] F. Billi, P. Campbell, Nanotoxicology of metal wear particles in total joint arthroplasty: a review of current concepts, J. Appl. Biomater. Biomech. 8 (1) (2010) 1–6.
[9] E. Ingham, J. Fisher, Biological reactions to wear debris in total joint replacement. Proc. Inst. Mech. Eng. H J. Eng. Med. 214 (1) (January 1, 2000) 21–37.
[10] J.R.T. Jeffers, W.L. Walter, Ceramic-on-ceramic bearings in hip arthroplasty: State of the art and the future, J. Bone Joint Surg. Br. Vol. 94-B (6) (June 1, 2012) 735–745.
[11] Arx Spinal System, US Food and Drug Administration (FDA), 510(k) number: K051525, 2006.
[12] Amedica/US Spine Enters the Reconstructive Surgery Market: First Silicon Nitride Total Hip Replacement http://www.amedicacorp.com/press_releases/amedica_us_spine_enters_the_reconstructive_surgery_market2011 (Published: 17 Feb 2011, Accessed: 6 Aug 2013).
[13] B.S. Bal, A. Khandkar, R. Lakshminarayanan, I.C. Clarke, A.A. Hoffman, M.N. Rahaman, Testing of silicon nitride ceramic bearings for total hip arthroplasty, J. Biomed. Mater. Res. B Appl. Biomater. 87B (2) (2008) 447–454.
[14] M. Herrmann, Corrosion of silicon nitride materials in aqueous solutions, J. Am. Ceram. Soc. 1–14 (2013).
[15] E. Laarz, B.V. Zhmud, L. Bergström, Dissolution and deagglomeration of silicon nitride in aqueous medium, J. Am. Ceram. Soc. 83 (10) (2000) 2394–2400.
[16] B.V. Zhmud, L. Bergström, Dissolution kinetics of silicon nitride in aqueous suspension, J. Colloid Interface Sci. 218 (2) (1999) 582–584.
[17] A. Neumann, M. Kramps, C. Ragoß, H.R. Maier, K. Jahnke, Histological and microradiographic appearances of silicon nitride and aluminum oxide in a rabbit femur implantation model*, Mater. Werkst. 35 (9) (2004) 569–573.
[18] T.J. Webster, A.A. Patel, M.N. Rahaman, B.S. Bal, Anti-infective and osteointegration properties of silicon nitride, poly-ether-ether-ketone, and titanium implants, Acta Biomater. 8 (12) (2012) 4447–4454.
[19] C.C. Guedes e Silva, O.Z. Higa, J.C. Bressiani, Cytotoxic evaluation of silicon nitride-based ceramics, Mater. Sci. Eng. C 24 (5) (2004) 643–646.
[20] C.C. Guedes e Silva, J.B. König, M.J. Carbonari, M. Yoshimoto, J.S. Allegrini, J.C. Bressiani, Bone growth around silicon nitride implants—an evaluation by scanning electron microscopy, Mater. Charact. 59 (9) (2008) 1339–1341.
[21] D.J. Gorth, S. Puckett, B. Ercan, T.J. Webster, M. Rahaman, B.S. Bal, Decreased bacteria activity on Si3N4 surfaces compared with PEEK or titanium, Int. J. Nanomedicine 7 (2012) 4829–4840 (eng).
[22] J. Olofsson, M. Pettersson, N. Teuscher, A. Heilmann, K. Larsson, K. Grandfield, et al., Fabrication and evaluation of Si_xN_y coatings for total joint replacements, J. Mater. Sci. Mater. Med. 23 (8) (2012) 1879–1889.
[23] M. Pettersson, T. Berlind, S. Schmidt, S. Jacobson, L. Hultman, C. Persson, et al., Structure and composition of silicon nitride and silicon carbon nitride coatings for joint replacements, Surf. Coat. Technol. 235 (0) (2013) 827–834.
[24] M. Pettersson, S. Tkachenko, S. Schmidt, T. Berlind, S. Jacobson, L. Hultman, et al., Mechanical and tribological behavior of silicon nitride and silicon carbon nitride coatings for total joint replacements, J. Mech. Behav. Biomed. Mater. 25 (2013) 41–47.
[25] C. Skjöldebrand, M. Pettersson, S. Schmidt, H. Högberg, H. Engqvist, C. Persson, Roughness and Mechanical Properties of Silicon Nitride Coatings – An Alternative for Joint Replacements, European Hip Society, Stockholm, Sweden, 2014.
[26] S.R. Brannan, D.A. Jerrard, Synovial fluid analysis, J. Emerg. Med. 30 (3) (2006) 331–339.
[27] D. Terčič, B. Božič, The basis of the synovial fluid analysis, Clin. Chem. Lab. Med. 39 (12) (2001) 1221.
[28] S.G. Moss, M.E. Schweitzer, J.A. Jacobson, J. Brossmann, J.V. Lombardi, S.M. Dellose, et al., Hip joint fluid: detection and distribution at MR imaging and US with cadaveric correlation, Radiology 208 (1) (1998) 43–48 (1998/07/01).
[29] M. Stern, A.L. Geary, Electrochemical polarization: I. A theoretical analysis of the shape of polarization curves, J. Electrochem. Soc. 104 (1) (January 1, 1957) 56–63.
[30] J.E.T. Hesketh, Tribocorrosion of Total Hip Replacements, the University Of Leeds, 2012.
[31] A. Sargeant, T. Goswami, Hip implants – Paper VI – ion concentrations, Mater. Des. 28 (1) (2007) 155–171.
[32] J. Black, Biological Performance of Materials: Fundamentals of Biocompatibility, fourth ed. CRC Press, 2005.
[33] B.K. Yen, R.L. White, R.J. Waltman, Q. Dai, D.C. Miller, A.J. Kellock, et al., Microstructure and properties of ultrathin amorphous silicon nitride protective coating, J. Vac. Sci. Technol., A 21 (6) (2003) 1895–1904.
[34] A.W.E. Hodgson, S. Kurz, S. Virtanen, V. Fervel, C.O.A. Olsson, S. Mischler, Passive and transpassive behaviour of CoCrMo in simulated biological solutions, Electrochim. Acta 49 (13) (2004) 2167–2178.
[35] I. Milošev, H.H. Strehblow, The composition of the surface passive film formed on CoCrMo alloy in simulated physiological solution, Electrochim. Acta 48 (19) (2003) 2767–2774.
[36] C. Pusch, H. Hoche, C. Berger, R. Riedel, E. Ionescu, A. Klein, Influence of the PVD sputtering method on structural characteristics of SiCN-coatings — comparison of RF, DC and HiPIMS sputtering and target configurations, Surf. Coat. Technol. 205 (2011) (S119-S23).
[37] W.-S. Cho, Y.-S. Oh, C.-S. Kim, M. Osada, M. Kakihana, D.-S. Lim, et al., Characterization of Si3N4/SiC nanocomposite by Raman scattering and XPS, J. Alloys Compd. 285 (1–2) (1999) 255–259.
[38] A.U. Alam, M.M.R. Howlader, M.J. Deen, Oxygen plasma and humidity dependent surface analysis of silicon, silicon dioxide and glass for direct wafer bonding, ECS J. Solid State Sci. Technol. 2 (12) (January 1, 2013) (P515-P23).
[39] D.-I. Kim, K.-H. Kim, H.-S. Ahn, Tribological properties of adsorbed water layer on silicon surfaces, Int. J. Precis. Eng. Manuf. 11 (5) (2010) 741–746 (2010/10/01, English).
[40] F. Pavlyák, I. Bertóti, M. Mohai, I. Biczó, J. Giber, AES and XPS characterization of SiNx layers, Surf. Interface Anal. 20 (3) (1993) 221–227.
[41] C.D. Wagner, W.M. Riggs, L.E. Davis, J.F. Maoulder, in: G.E. Mulienberg (Ed.), Handbook of X-ray Photoelectron Spectroscopy: A Reference Book of Standard Data for Use in X-ray Photoelectron Spectroscopy, Physical Electronics Division, Perkin-Elmer Corp., 1979
[42] J.M. Maloney, S.A. Lipka, S.P. Baldwin, In vivo biostability of CVD silicon oxide and silicon nitride films. Mater, Res. Soc. Symp. Proc. 872 (J14.3) (2005) 1–6.
[43] J.F. Hetke, J.L. Lund, K. Najafi, K.D. Wise, D.J. Anderson, Silicon ribbon cables for chronically implantable microelectrode arrays, IEEE Trans. Biomed. Eng. 41 (4) (1994) 314–321.
[44] Y.T. Konttinen, M. Takagi, J. Mandelin, J. Lassus, J. Salo, M. Ainola, T.F. Li, et al., Acid attack and cathepsin K in bone resorption around total hip replacement prosthesis, J. Bone Miner. Res 16 (10) (2001) 1780–6. (eng).
[45] S. Karimi, T. Nickchi, A. Alfantazi, Effects of bovine serum albumin on the corrosion behaviour of AISI 316L, Co–28Cr–6Mo, and Ti–6Al–4V alloys in phosphate buffered saline solutions, Corros. Sci. 53 (10) (2011) 3262–3272.
[46] J. Lutz, C. Díaz, J.A. García, C. Blawert, S. Mändl, Corrosion behaviour of medical CoCr alloy after nitrogen plasma immersion ion implantation, Surf. Coat. Technol. 205 (8–9) (2011) 3043–3049.
[47] M. Metikoš-Huković, R. Babić, Passivation and corrosion behaviours of cobalt and cobalt–chromium–molybdenum alloy, Corros. Sci. 49 (9) (2007) 3570–3579.
[48] A. Igual Muñoz, S. Mischler, Effect of the environment on wear ranking and corrosion of biomedical CoCrMo alloys, J. Mater. Sci. Mater. Med. 22 (3) (2011) 437–450 (2011/03/01, English).
[49] J. Xu, K. Kato, Formation of tribochemical layer of ceramics sliding in water and its role for low friction, Wear 245 (1–2) (2000) 61–75.
[50] A. Kundra, A. Jain, A. Banga, G. Bajaj, P. Kar, Evaluation of plasma ammonia levels in patients with acute liver failure and chronic liver disease and its correlation with the severity of hepatic encephalopathy and clinical features of raised intracranial tension, Clin. Biochem. 38 (8) (2005) 696–699.
[51] J.A. Dean, Lange's Handbook of Chemistry, 15th ed. McGraw-Hill Inc., US, 1999.